Supporting Information

Efficient and stable organic solar cells based on metal oxide as all charge transport layers

Yangdan Tao, Di Wang, Xinyu He, Hongzheng Chen and Chang-Zhi Li*

Y. Tao, D. Wang, X. He, Prof. H. Chen and Prof. C-Z. Li
State Key Laboratory of Silicon and Advanced Semiconductor Materials, Department of Polymer Science and Engineering, Zhejiang University, Hangzhou 310027, P. R. China.
E-mail: czli@zju.edu.cn

1. General Information

Materials

All reagents and solvents, unless otherwise specified, were purchased from commercial sources and were used without further purification.

Characterization

EPR spectra were recorded at room temperature on a Bruker A300 X-band EPR spectrometer.

The conductivities of the different HTLs were measured with the structure of ITO/HTLs/Ag. The direct current conductivity (σ_0) can be calculated from the slope of *I-V* curves, using the equation $I = \sigma_0 A d^{-1} V$, where d is the thickness of the thin films and A is the area of sample (5.979 mm^2).

Ultraviolet photoemission spectroscopy (UPS) and X-ray photoelectron spectroscopy (XPS) measurements were obtained on PHI 5000 VersaProbe III. The valence-band (VB) spectra were referenced to the Fermi level (E_F = 0) determined from the thick metal films on the sample. A sample bias of −5 V was applied to observe the secondary electron cutoff. The work function (W_Φ) is determined by the difference between the photon energy and the binding energy of the secondary cutoff edge ($W_\Phi = h\nu - E_{cutoff} + E_F$).

Height and phase images of films were obtained on a VeecoMultiMode Atomic Force

Microscopy (AFM) in the tapping mode used an etched silicon cantilever at a nominal load of ~2 nN, and the scanning rate for a 2 μm×2 μm image size was 1.5 Hz.

The field-emission scanning electron microscope (FESEM) measurements were carried out on Scios2 Hivac.

Contact angle was characterized by OSA™ Optical Surface Analyzer SurfaceMeter™ from Ningbo NB Scientific Instruments Co.,Ltd.

UV-vis-NIR absorption spectra were recorded on a HITACHI U-4100 spectrophotometer.

GIWAXS measurements were carried out with Xeuss 2.0 using a Cu X-ray source (1.54 Å) and an Pilatus3R 300K detector. The incidence angle is ~0.2°.

The current density-voltage (*J-V*) curves of photovoltaic devices were measured in the glovebox with Keithley 2400, under AM 1.5G illumination at 100 mW cm^{-2} irradiation using an Enli SS-F5-3A solar simulator, and the light intensity was calibrated with a standard Si solar cell with KG5 filter (made by Enli Technology Co., Ltd., Taiwan, and calibrated report can be traced to NREL).

The external quantum efficiency (EQE) spectrum was measured using a QE-R Solar Cell Spectral Response Measurement System (Enli Technology Co., Ltd., Taiwan).

The charge carrier mobilities of OSC device with different HTLs were measured using the space-charge-limited current (SCLC) method. Hole-only devices are conducted with the structure of ITO/HTLs/PM6:Y6/HTLs/Ag. The device charac-teristics were extracted by modeling the dark current under forwarding bias using the SCLC expression described by the Mott-Gurney law:

$$J = \frac{9}{8}\varepsilon_r\varepsilon_0\mu\frac{V^2}{L^3}$$

The photostability of devices measured in air (70 % humidity) under encapsulation. An array of white LEDs was used as light source with intensity equivalent to 1 sun, which was calibrated by matching the device performance to the measured under AM 1.5 G. The initial exposure time is defined as time 0 s. The devices were kept under open-circuit conditions. The temperature of the cells was 20-30 °C during measurements.

2. Synthesis of MOs

Synthesis of I-MoO_x

150 mg of MoO_3 powders and 3 mL of aqueous hydrogen peroxide were added into deionized water (15 mL). The mixture was dissolved by sonication to obtain yellow solution. And then remove the solvents by vacuum rotary evaporator to afford orange powder (MoO_x). Finally, the MoO_x powders were diluted in deionized water (10 mg mL^{-1}) and methylammonium iodide (MAI) was introduced to the solution in a weight ratio of 3wt% to formulate I-MoO_x.

Synthesis of S3-ZnO NPs

The synthesis of S3-ZnO NPs can be found in our previous work.[1] Zinc acetate dihydrate (2.95 g) was dissolved in methanol (125 mL) at 60 ℃ under stirring. Potassium hydroxide (1.48 g) in methanol (65 mL) was added to the zinc acetate solution. The reaction mixture was stirred at 60 ℃ for 3 h. After reaction, the solution was stored overnight and then zinc oxide precipitates were collected and washed by methanol for three times. Finally, zinc oxide nanoparticles (ZnO NPs) were dispersed in ethanol (10 mg mL-1). Small molecules, S3 were added to the ZnO NPs suspension in a weight ratio of 1: 10 (S3/ZnO) and the mixture was stirred overnight to formulate S3-ZnO NPs.

3. Fabrication of OSCs.

The conventional device architecture was ITO/HTLs/Active layer/S3-ZnO NPs/Ag. The glass/ITO substrates were cleaned by sonication using detergent, deionized water, acetone, and isopropanol sequentially for 30 min before fabrication. The pre-cleaned ITO substrates were then treated in an ultraviolet generator for 30 min.

Fabrication of hole transport layers

The MoO_x or I-MoO_x layer were deposited from 10 mg mL^{-1} of deionized water at 3300 rpm for 30 s and then annealing at 150 ℃ for 20 min. The PEDOT: PSS (Clevios™ P VP Al 4083) layer was deposited at 45000 rpm and then annealing at 150 ℃ for 20 min. The MoO_3 layer with different thickness was deposited by thermal evaporation under a background pressure of approximately 2.0×10^{-4} Pa. Then the substrates were transferred into a glovebox.

Fabrication of active layers

PM6:Y6 (1: 1.2 weight ratio) blends were spin-coated from 16.5 mg mL^{-1} chloroform with 0.5 vol.% 1-chloronaphthalene (CN) at 3000 rpm for 30 s to form active layers and then annealing at 90 ℃ for 7 min. PM6:L8-BO (1: 1.2 weight ratio) blends were spin-coated from 16 mg mL^{-1} chloroform with 0.25 vol.% 1,8-diiodooctane (DIO) at 3500 rpm for 30 s to form active layers and then annealing at 90 ℃ for 7 min. P3HT:$PC_{71}BM$ (1: 0.8 weight ratio) blends were spin-coated from 40 mg mL^{-1} chlorobenzene at 2500 rpm for 30 s to form active layers and then annealing at 140 ℃ for 7 min. PTB7:$PC_{71}BM$ (1: 1.5 weight ratio) blends were spin-coated from 25 mg mL^{-1} chlorobenzene with 3 vol.% 1,8-diiodooctane (DIO) at 1400 rpm for 30 s to form active layers.

Fabrication of electron transport layers

The S3-ZnO NPs layers were deposited from 5 mg mL^{-1} of ethanol solution at 3000 rpm for 30 s to obtain the electron transport layer of 30 nm, followed by thermal annealing at 90 ℃ for 3 min.

Fabrication of electrode

Ag electrode with a thickness (100 nm) was deposited by thermal evaporation under a background pressure of approximately 2.0×10^{-4} Pa, to complete the device with an active area of 9.25 mm^2. All OSCs were measured with a mask (5.979 mm^2).

4. Supporting figures

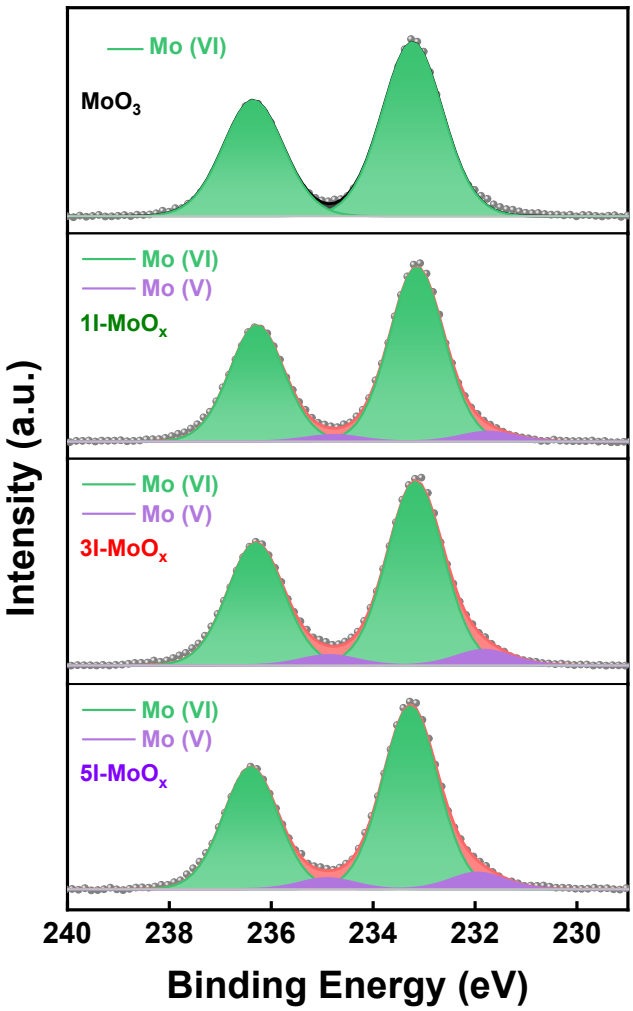

Figure S1. XPS spectra of MoO_x and different concentration MAI doped MoO_x.

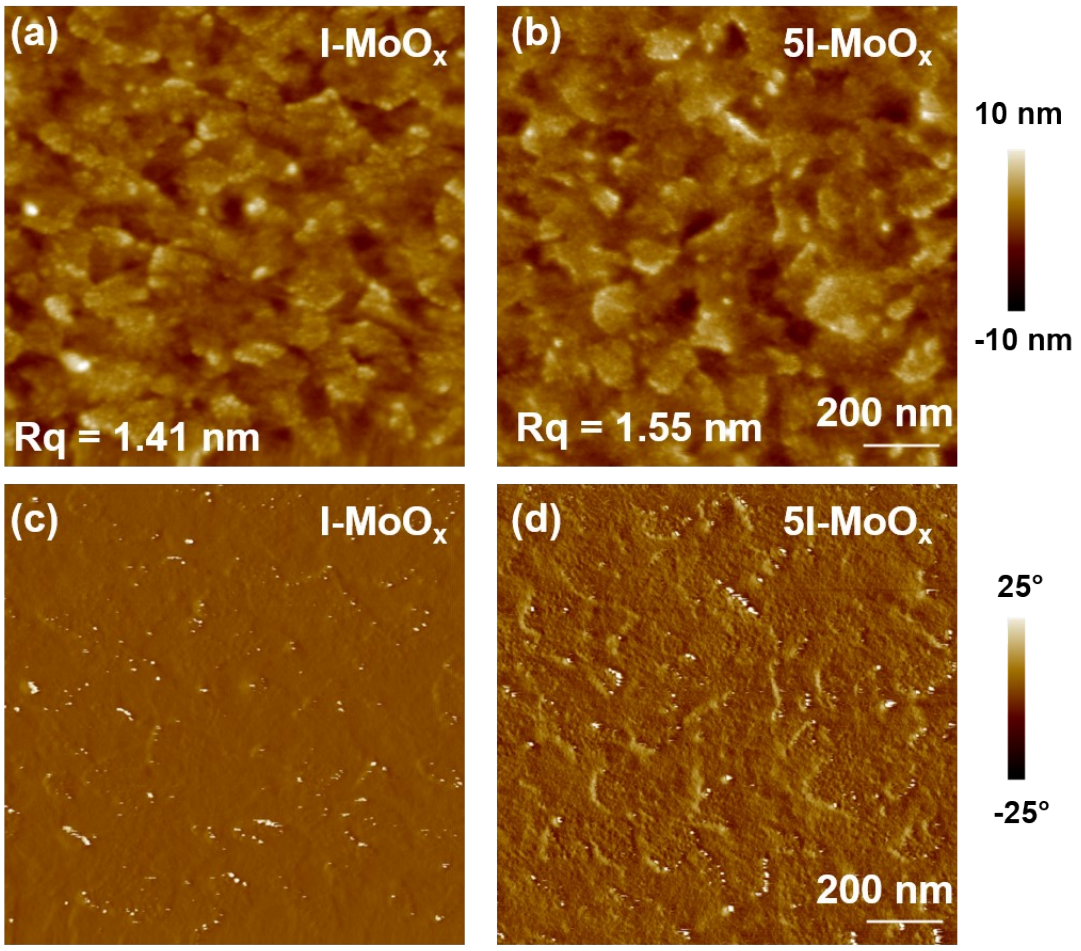

Figure S2. AFM (a-b) height and (c-d) phase images of I-MoO_x (3wt% MAI doped MoO_x) and 5I-MoO_x (5wt% MAI doped MoO_x).

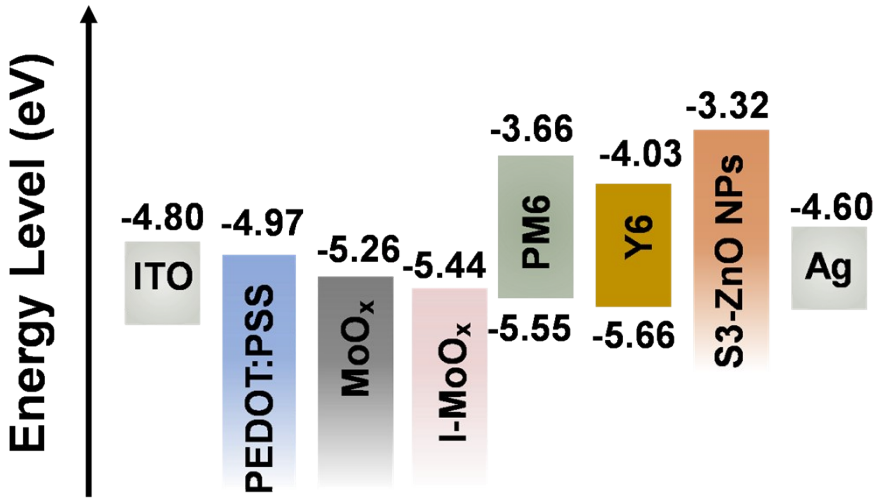

Figure S3. The energy level diagram of each component used in devices.

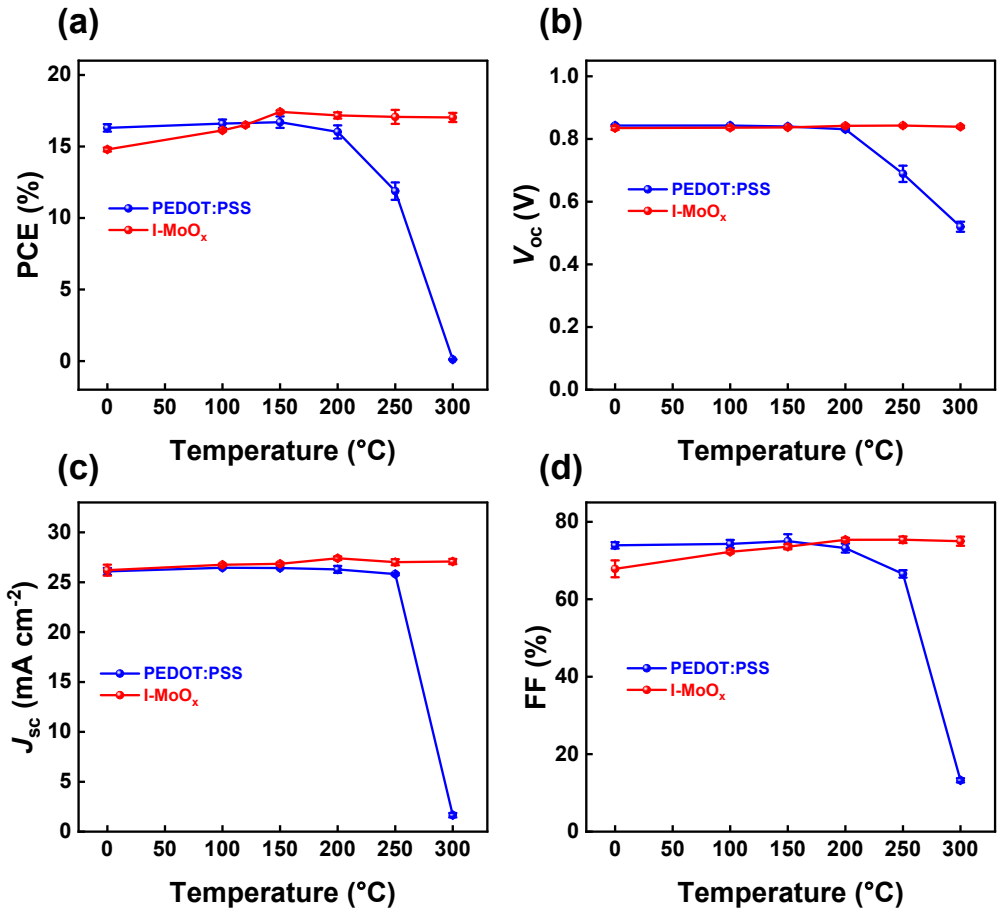

Figure S4. a) PCE, b) V_{oc}, c) J_{sc} and d) FF of OSCs based on MoO_x and PEDOT:PSS as a function of HTLs annealing temperature.

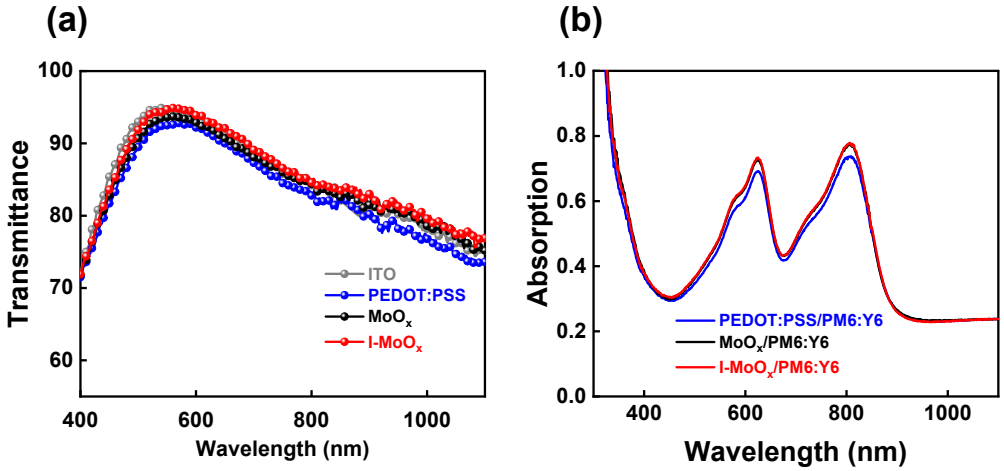

Figure S5. a) Transmittance spectra of different HTLs and b) normalized absorption spectra of PM6:Y6 blends coated on different HTLs.

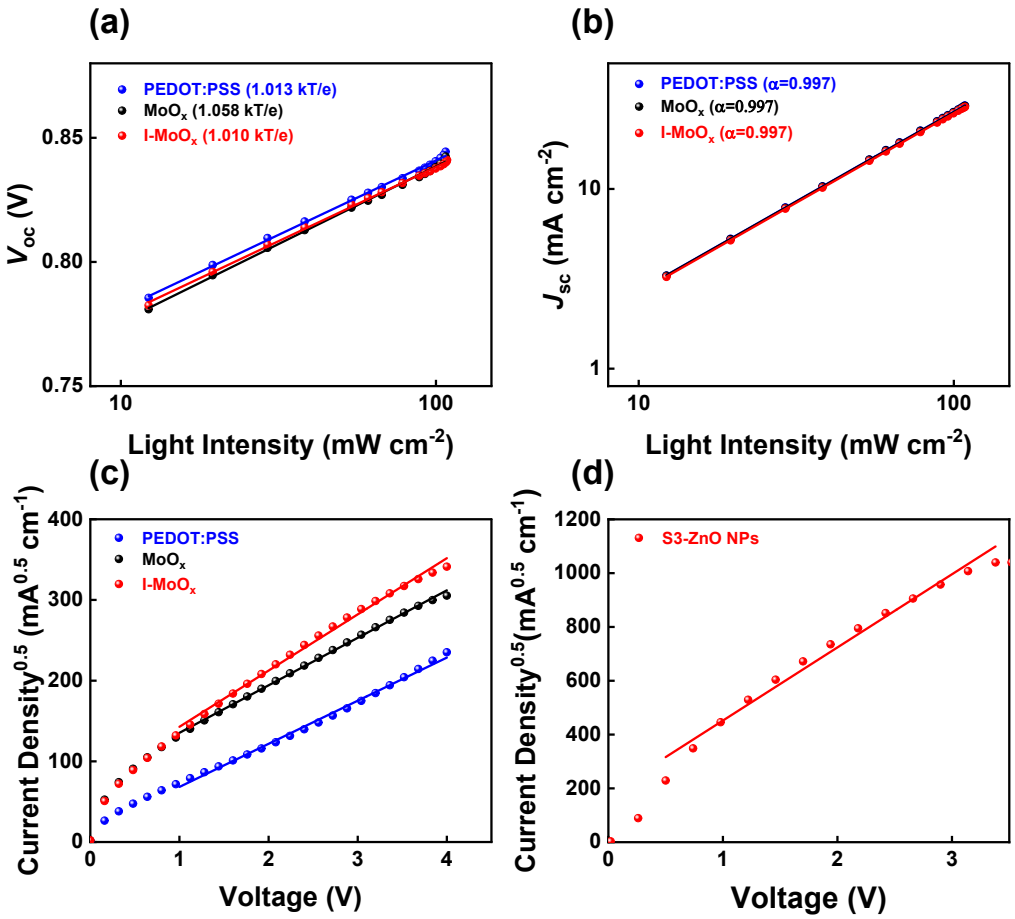

Figure S6. a) V_{oc}; b) J_{sc} values as a function of light intensity; $J^{0.5}$-V curves of the c) hole-only devices with a structure of ITO/HTLs/PM6:Y6/HTLs/Ag and d) electron-only devices with a structure of ITO/ETLs/PM6:Y6/ETLs/Ag.

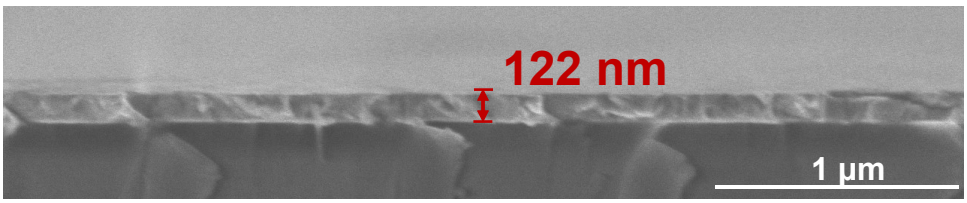

Figure S7. The cross-section SEM image of I-MoO_x from the solution concentration and spin coating speed of 40 mg mL^{-1} and 2000 rpm.

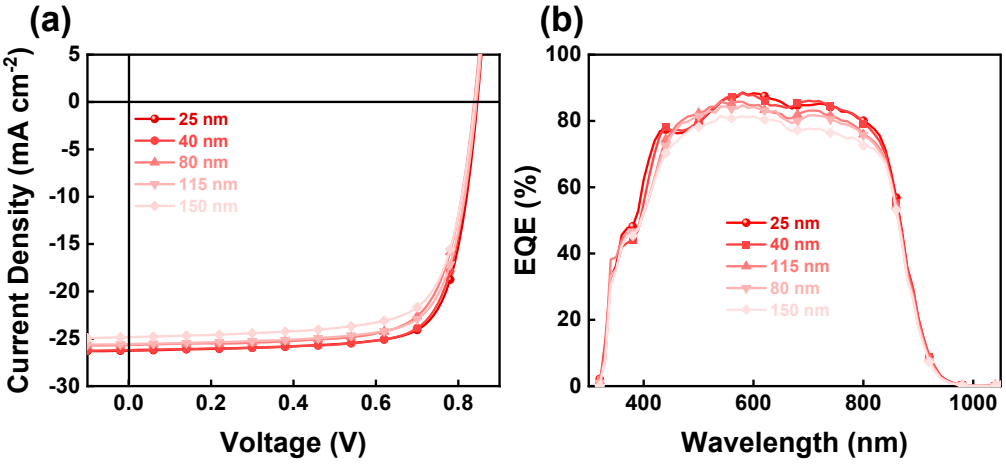

Figure S8. a) *J-V* curves and b) EQE spectra of OSCs based on I-MoO_x HTLs with different thickness.

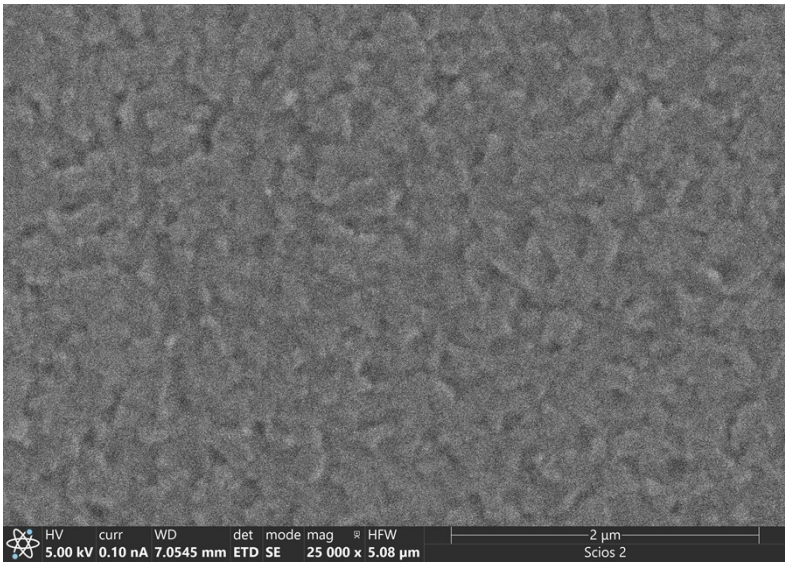

Figure S9. The SEM image of I-MoO_x films.

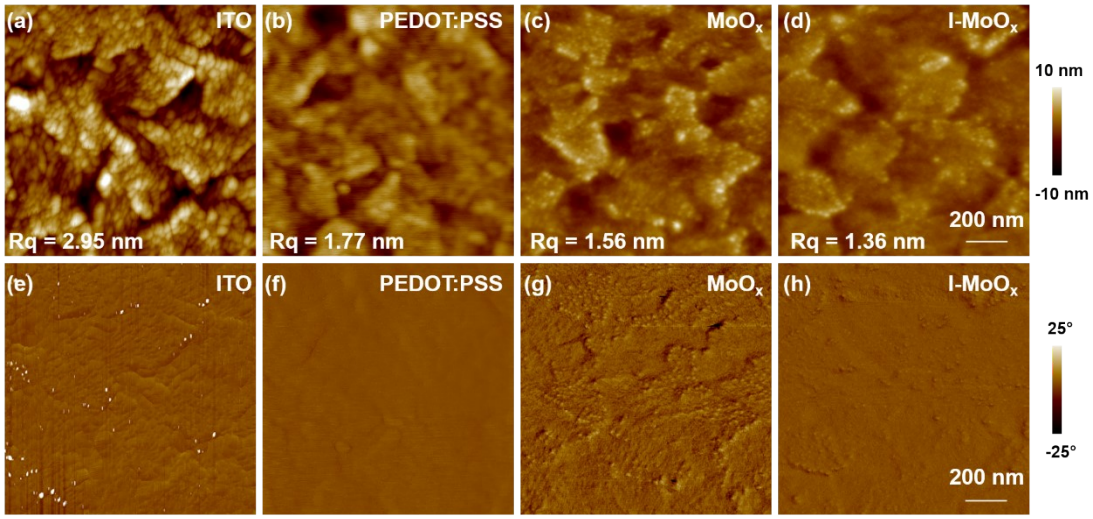

Figure S10. AFM (a-d) height and (e-h) phase images of different HTLs.

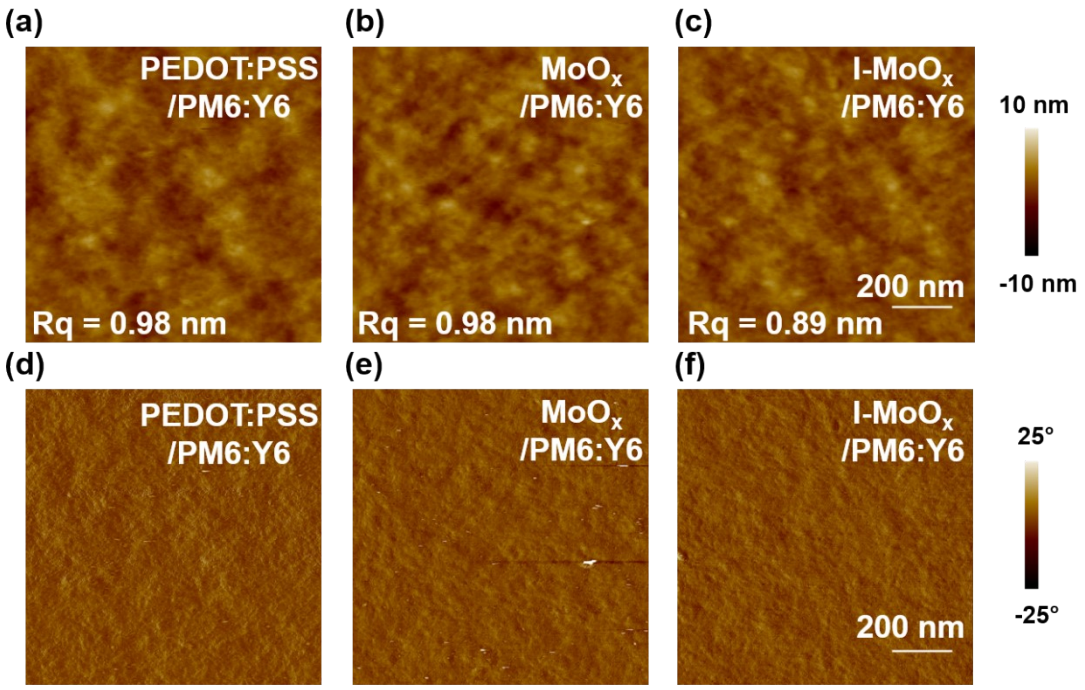

Figure S11. AFM (a-c) height and (d-f) phase images of PM6:Y6 blends on top of different HTLs.

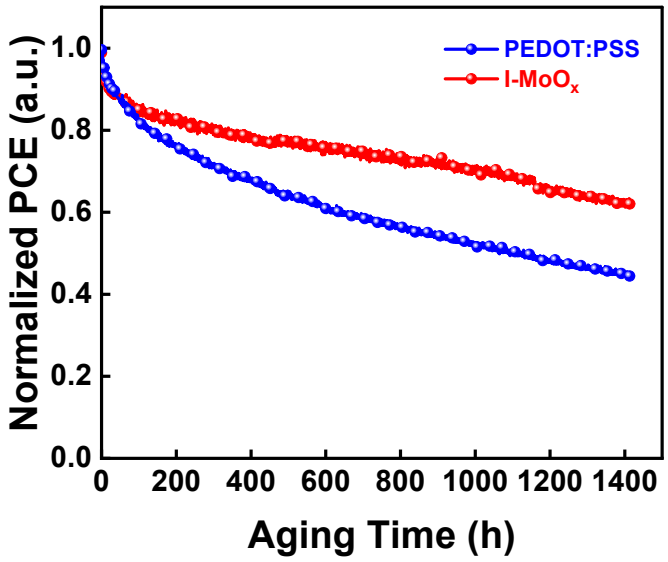

Figure S12. Photo stabilities of PEDOT:PSS and I-MoO_x devices based on PM6:Y6 BHJ layers under maximum power point (MPP) conditions (1 sun equivalent illumination).

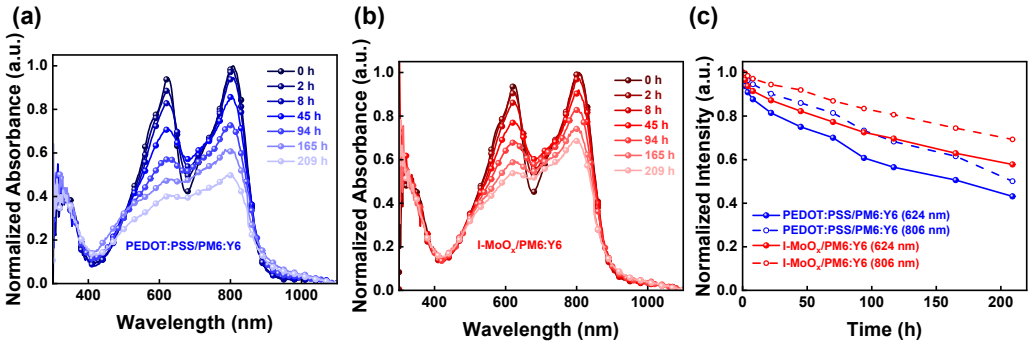

Figure S13. Absorption spectra of a) PEDOT:PSS/PM6:Y6 and b) I-MoO_x/PM6:Y6 films under one-sun equivalent illumination in ambient; c) the change of absorption intensity versus photoaging time.

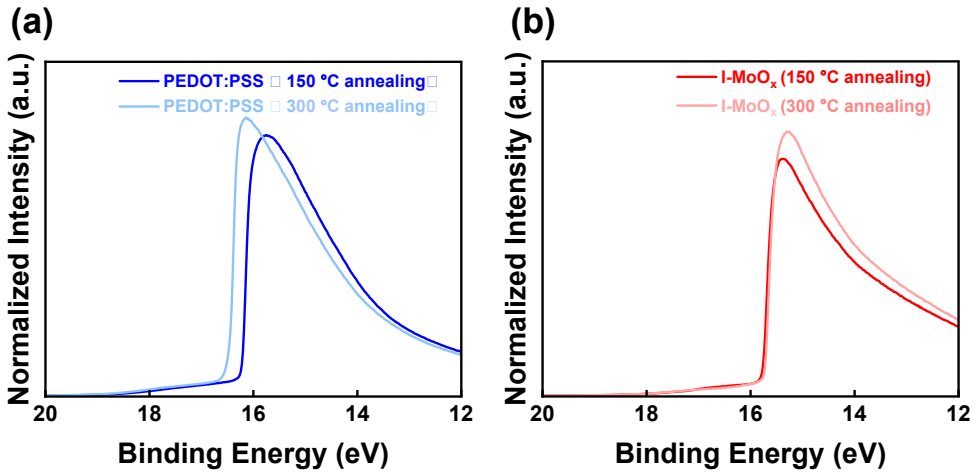

Figure S14. Work function measurments of the (a) PEDOT:PSS/ITO and (b) I-MoO_x/ITO for 150 ℃ and 300 ℃ annealing temperature, respectively.

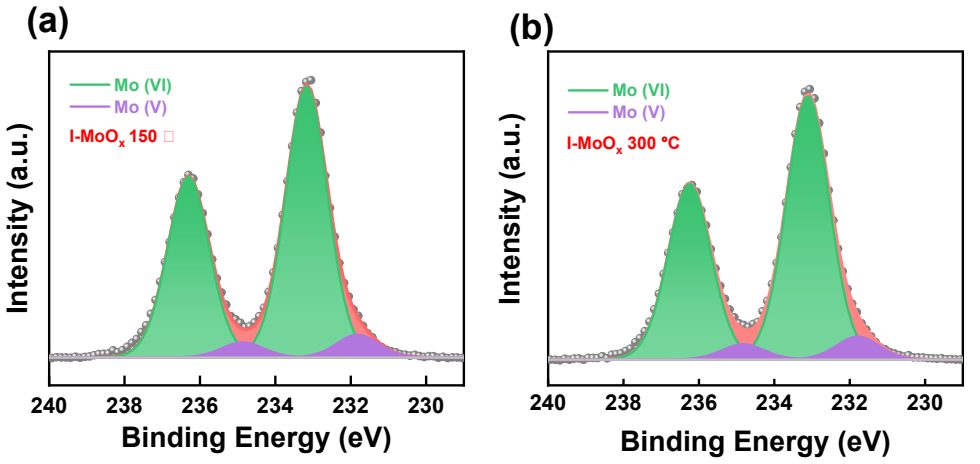

Figure S15. XPS spectra of the I-MoO_x with (a) 150 ℃ annealing and (b) 300 ℃ annealing.

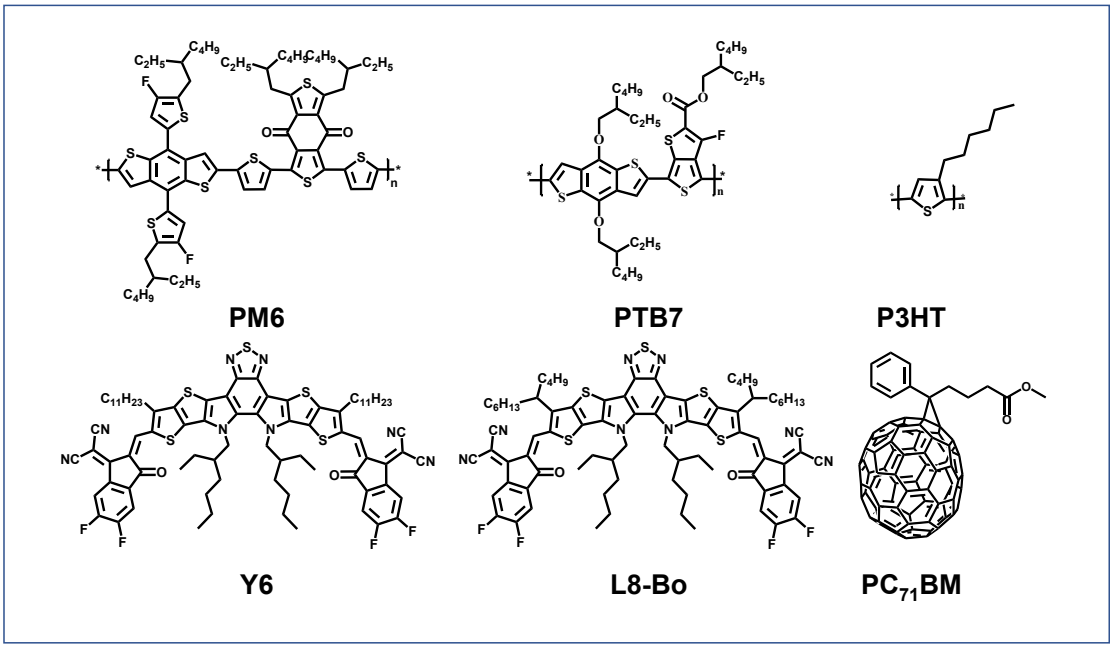

Figure S16. Chemical structure of photovoltaic donors and acceptors used in this study.

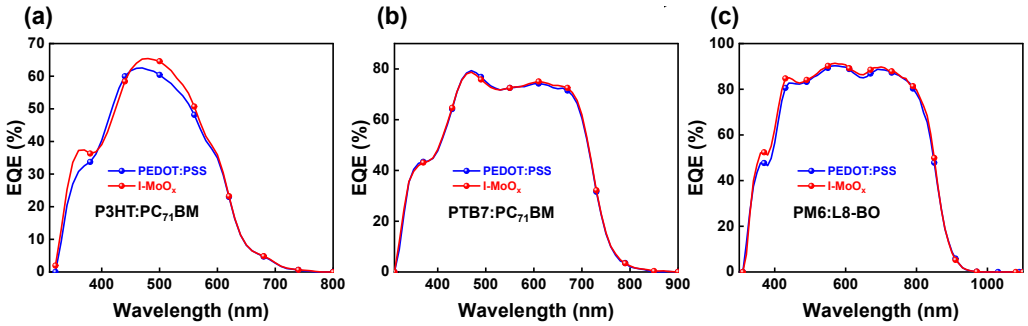

Figure S17. EQE spectra of OSCs with different BHJ based on PEDOT:PSS or I-MoO_x HTLs.

5. Supporting Tables

Table S1. The correlation between device performance, conductivities and Mo (V) concentration in doped I-MoO_x.

Sample	Mo (V) concentration (%)	σ_0 ($\times 10^{-4}$ S m^{-1})	PCE (%)
MoO_x	0.00	6.47±0.93	17.0 (16.7 ± 0.2)
1I-MoO_x	5.37	8.97±1.69	17.2 (17.1 ± 0.1)
3I-MoO_x	7.79	10.00±1.35	17.7 (17.4 ± 0.1)
5I-MoO_x	8.36	6.43±0.95	16.7 (16.5 ± 0.1)

Table S2. The work function of the PEDOT:PSS, MoO_x and I-MoO_x.

Sample	WF (eV)
PEDOT:PSS	4.97
MoO_x	5.26
I-MoO_x	5.44

Table S3. Device performance of the PM6:Y6 OSCs with different annealing temperature for I-MoO_x HTLs.

Temperature (℃)	V_{oc} [V]	J_{sc} [mA cm^{-2}]	FF [%]	PCE [%]
0	0.824 (0.835 ± 0.006)	25.6 (26.2 ± 0.6)	71.8 (67.9 ± 2.2)	15.2 (14.8 ± 0.1)
100	0.843 (0.836 ± 0.005)	26.9 (26.8 ± 0.1)	72.0 (72.3 ± 0.4)	16.2 (16.1 ± 0.1)
120	0.837 (0.837 ± 0.003)	27.0 (26.9 ± 0.1)	74.0 (73.6 ± 0.7)	16.7 (16.5 ± 0.1)
150	0.848 (0.847 ± 0.003)	27.5 (27.4 ± 0.2)	75.4 (75.4 ± 0.5)	17.7 (17.4 ± 0.1)
200	0.847 (0.844 ± 0.003)	27.1 (27.0 ± 0.3)	76.0 (75.4 ± 0.9)	17.5 (17.2 ± 0.2)
250	0.846 (0.839 ± 0.004)	27.4 (27.1 ± 0.3)	75.9 (75.0 ± 1.2)	17.6 (17.1 ± 0.5)
300	0.842 (0.833 ± 0.004)	27.3 (27.1 ± 0.4)	75.2 (74.9 ± 0.7)	17.5 (17.0 ± 0.3)

Table S4. Device performance of the conventional PM6:Y6 OSCs with different hole transport layers.

	V_{oc} [V]	J_{sc} [mA cm^{-2}]	$J_{cal.}$ [mA cm^{-2}]	FF [%]	PCE [%]
PEDOT:PSS	0.849 (0.847 ± 0.002)	26.8 (27.0 ± 0.2)	26.4	75.9 (75.1 ± 0.9)	17.3 (17.1 ± 0.1)
MoO_x	0.849 (0.845 ± 0.003)	26.4 (26.7 ± 0.2)	25.8	75.8 (74.2 ± 1.0)	17.0 (16.7 ± 0.2)
1I-MoO_x	0.845 (0.843 ± 0.002)	27.2 (26.9 ± 0.3)	26.3	75.0 (75.1 ± 0.7)	17.2 (17.1 ± 0.1)
3I-MoO_x	0.848 (0.847 ± 0.003)	27.5 (27.2 ± 0.3)	26.6	75.4 (75.6 ± 0.5)	17.7 (17.4 ± 0.1)
5I-MoO_x	0.844 (0.844 ± 0.003)	26.6 (26.7 ± 0.2)	26.1	74.8 (73.5 ± 0.9)	16.7 (16.5 ± 0.1)

Table S5. Device performance of the PM6:Y6 OSCs with different thicknesses of I-MoO_x HTLs.

Thickness (nm)	V_{oc} [V]	J_{sc} [mA cm^{-2}]	$J_{cal.}$ [mA cm^{-2}]	FF [%]	PCE [%]
25	0.846 (0.842 ± 0.004)	26.3 (26.7 ± 0.3)	26.2	76.1 (73.9 ± 1.4)	16.9 (16.6 ± 0.2)
40	0.843 (0.842 ± 0.004)	26.2 (26.4 ± 0.4)	26.0	75.8 (73.7 ± 1.8)	16.7 (16.4 ± 0.3)
80	0.838 (0.838 ± 0.003)	25.7 (25.6 ± 0.4)	25.5	73.7 (72.5 ± 0.9)	15.8 (15.5 ± 0.3)
115	0.844 (0.839 ± 0.003)	25.6 (25.6 ± 0.3)	25.1	74.4 (73.3 ± 0.8)	16.0 (15.7 ± 0.2)
150	0.840 (0.831 ± 0.004)	24.8 (24.7 ± 0.1)	24.2	72.8 (72.3 ± 0.5)	15.2 (14.8 ± 0.2)

Table S6. Device performance of the PM6:Y6 OSCs with different thicknesses of MoO_x HTLs.

Thickness (nm)	V_{oc} [V]	J_{sc} [mA cm^{-2}]	FF [%]	PCE [%]
25	0.840 (0.841 ± 0.001)	26.0 (26.1 ± 0.1)	75.8 (74.1 ± 1.2)	16.5 (16.3 ± 0.2)
40	0.823 (0.823 ± 0.003)	25.8 (25.9 ± 0.2)	71.7 (70.8 ± 0.4)	15.2 (15.1 ± 0.1)
80	0.828 (0.830 ± 0.003)	25.7 (25.9 ± 0.1)	66.2 (65.2 ± 0.6)	14.1 (14.0 ± 0.1)
115	0.825 (0.824 ± 0.002)	25.3 (25.4 ± 0.2)	65.0 (64.7 ± 0.4）	13.6 (13.5 ± 0.0)
150	0.824 (0.82 ± 0.001)	25.2 (25.3 ± 0.1)	61.1 (59.8 ± 1.0)	12.7 (13.5 ± 0.2)

Table S7. Performance of the PM6:Y6 OSCs with different thicknesses of pristine MoO_3 HTLs via thermal evaporation.

Thickness (nm)	V_{oc} [V]	J_{sc} [mA cm^{-2}]	FF [%]	PCE [%]
8	0.844 (0.840 ± 0.002)	26.3 (26.0 ± 0.2)	77.0 (77.1 ± 0.2)	17.1 (16.8 ± 0.2)
25	0.841 (0.839 ± 0.002)	26.1 (25.9 ± 0.1)	75.7 (75.6 ± 0.6)	16.6 (16.4 ± 0.2)
50	0.838 (0.840 ± 0.004)	25.5 (25.6 ± 0.1)	75.6 (73.9 ± 1.2)	16.1 (15.9 ± 0.2)
100	0.841 (0.840 ± 0.002)	24.8 (24.2 ± 1.1)	61.6 (57.2 ± 2.8)	12.8 (11.6 ± 0.6)
150	0.844 (0.839 ± 0.003)	23.1 (23.6 ± 1.2)	53.0 (48.9 ± 3.1)	10.3 (9.7 ± 0.4)

Table S8. OSCs with different thickness of HTLs in references.

Years	Devices Structure	CILs	Thickness (nm)	PCE (%)	Ref
2018	ITO/CILs/PB3T2:IT-M/PFN-Br/Al	H-V:Mo	10 30 65 85 110 150	11.40 10.50 9.70 9.30 8.10 7.60	2
2018	ITO/CILs/PB3T:IT-M/PFN-Br/Ag	EG:Mo	5 10 30 60 80 100 130 150 190	11.40 12.10 11.50 11.30 10.60 9.65 9.15 8.83 7.95	3
2018	ITO/CILs/PM6:IT-4F/PFN-Br/Al	WO_x:PEDOT:PSS	22 35 42 58 65	13.48 14.33 14.57 14.16 13.95	4
2019	ITO/CILs/PBDBT-2F:IT-4F/PFN-Br/Al	PCP-2F-Li	4 7 10 15 20 25	12.20 12.70 12.50 12.00 11.70 11.20	5

			30	10.50	
2019	ITO/CILs/PBDB-T:ITIC/PFN/Ag	PEDOT:PDAS	15 30 40 55	9.75 9.55 9.42 9.32	6
2020	ITO/CILs/PM6:BTP-4F-12/PFNDIT-F3N/Ag	PDAS	30 40 50	16.00 16.20 15.80	7
2020	ITO/CILs/PBDB-T-2F:Y6/PFN-Br/Al	PMC-4	5 20 40	16.34 14.24 13.47	8
2020	ITO/CILs/PM6:Y6/PFN/Al	$PCPDTK_{0.5}H_{0.5}$-TT	5 10 20 30 40 50 60	16.80 17.00 16.70 15.90 14.60 12.70 11.80	9
2021	ITO/CILs/PM6:BTP-eC9/PFN-Br/Ag	HPMO:Sn	10 30 40 50	17.14 16.11 15.08 14.22	10
2022	ITO/CILs/PM6:BTPBO-4Cl/PFN-Br/Ag	Cu003	6 9 12 15	17.60 16.90 14.50 12.70	11
2022	ITO/CILs/PB3T:IT-M/PFN-Br/Al	G:Mo	10 100	11.12 8.31	12
2022	ITO/CILs/PM6:L8-BO/PFNDI-Br/Ag	Co-La50%	3 5 10 20	18.08 18.82 17.62 17.41	13
2022	ITO/PEI-ZnO/PM6:Y6:$PC_{71}BM$/CILs/Ag	PEDOT:F	15 25 40 50 65	15.97 16.15 16.28 16.16 15.89	14

Table S9. Detailed parameters of GIWAXS profiles for PM6:Y6 blends on top of different HTLs.

HTLs	(100) Out of plane				(010) In plane			
	q ($Å^{-1}$)	d (Å)	FWHM ($Å^{-1}$)	CCL (Å)	q ($Å^{-1}$)	d (Å)	FWHM ($Å^{-1}$)	CCL (Å)
PEDOT:PSS	0.32	19.63	0.10	62.83	1.82	3.45	0.33	19.04
MoO_3	0.32	19.63	0.10	62.83	1.82	3.45	0.34	18.48
I-MoOx	0.32	19.63	0.09	69.81	1.82	3.45	0.33	19.04

Table S10. Device performance of the PM6: Y6 OSCs with different annealing temperature for PEDOT:PSS HTLs.

Temperature (℃)	V_{oc} [V]	J_{sc} [mA cm^{-2}]	FF [%]	PCE [%]
0	0.846 (0.84 ± 0.003)	25.9 (26.1 ± 0.4)	75.7 (73.9 ± 0.8)	16.7 (16.3 ± 0.3)
100	0.847 (0.843 ± 0.002)	26.6 (26.5 ± 0.1)	75.3 (74.3 ± 1.1)	17.0 (16.6 ± 0.3)
150	0.843 (0.840 ± 0.003)	26.4 (26.4 ± 0.1)	77.0 (75.0 ± 1.8)	17.2 (16.7 ± 0.4)
200	0.835 (0.831 ± 0.003)	26.8 (26.3 ± 0.4)	74.7 (73.2 ± 1.2)	16.8 (16.0 ± 0.5)
250	0.727 (0.690 ± 0.026)	25.9 (25.8 ± 0.1)	68.5 (66.6 ± 1.0)	12.9 (11.9 ± 0.6)
300	0.545 (0.520 ± 0.020)	2.08 (1.65 ± 0.22)	14.4 (13.3 ± 0.6)	0.164 (0.115 ± 0.022)

Table S11. PCEs for OSCs based on all metal oxide transport layers between this work and references.

Years	Devices Structure	PCE (%)	Ref.
2019	ITO/AZO:PDA/PM6:IT-4F/MoO_3/Ag	12.70	15
2019	ITO/ZnO/SAM1/PM6:IT-4F/MoO_3/Ag	13.25	16
2019	ITO/ZnO/PM6:Y6/MoO_3/Ag	15.70	17
2020	ITO/ZnO/PM6:Y6:$PC_{71}BM$/MoO_3/Ag	16.63	18
2020	ITO/aq-MoOx/PM6:Y6/ZnO NP/Ag	17.00	19
2020	ITO/an-MoOx/PM6:Y6/ZnO NP/Ag	17.10	19
2021	ITO/ZnO/PM7:IT-4F/SL-HMoOx/Al	13.17	20
2021	ITO/ZnO/PBDB-T:PhO4T-3/MoO_3/Ag	13.76	21
2021	ITO/ZnO/PTzBI-*d*F:CH1007:PC71BM/MoO_3/Ag	15.10	22
2021	ITO/ZnO/PM6:Y6/s-MoOx/Ag	15.20	23
2021	ITO/ZnO/PET/PM6:Y6/MoO_3/Ag	16.46	24
2021	ITO/ZnO/PM6:Y6/SC-HMoOx/Al	16.58	20
2021	ITO/ic-ZnO/PM6:Y6/MoO_3/Al	16.62	25
2021	ITO/ZnO/PM6:Y6/DBC-HMoOx/Al	16.64	20
2021	ITO/AZO/PM6:L8-BO-F:Y6-BO/MoO_3/Ag	17.46	26
2021	ITO/AZO/PM6:Y6:BTO:$PC_{71}BM$/MoO_3/Al	17.48	26
2021	ITO/ZnO:Zr/PM6:BTP-eC9/MoO_3/Ag	17.70	27
2022	ITO/ZnO/PM6:Y6/s-MoO_x/Ag	16.28	28
2022	ITO/ZnO/TPIZ/PM6:Y6/MoO_3/Ag	16.37	29
2022	ITO/ZnO/PM6:BTP-eC9/MoO_3/Ag	16.47	30
2022	ITO/ZnO/P4VP/PM6:CH1007:PC71BM/MoO_3/Ag	16.56	31
2022	ITO/CD/PM6:Y6:PC71BM/MoO3/Ag	16.80	32
2022	ITO/PEI-ZnO/PM6:PC71BM:BTP-eC9/MoO_3/Ag	16.81	14
2022	ITO/ZnO/PET/PM6:L8-BO/MoO_3/Al	17.02	33
2022	ITO/ZnO/PM6:L8-BO/s-MoO_x/Ag	17.12	28
2022	ITO/SnO2:PAS/PM6:BTP-eC9/MoO_3/Ag	17.12	34
2022	ITO/CD/PM6:BTP-eC9/MoO_3/Ag	17.35	32
2022	ITO/ZnO/NMA/PM6:Y6:$PC_{71}BM$/MoO_3/Ag	17.41	35
2022	ITO/PA-ZnO/PM6:BTP-eC9/MoO_x/Ag	17.60	36
2022	ITO/ZnO/NMA/PM6:L8-BO/MoO_3/Ag	17.68	35
2022	ITO/SnO2/1-DPAQ/PM6:BTP-eC9/MoO_3/Ag	17.70	37
2022	ITO/SnO2/1-DPAQ/PM6:PB2F:BTP-eC9/MoO_3/Ag	18.10	37
2022	ITO/ZnO/NMA/D18:N3/MoO_3/Ag	18.20	35
2022	ITO/AZO/PM6:L8-BO-F:Y6-BO/2PACz/MoO_3/Ag	18.49	38
2023	ITO/ZnO/PQSi705:Y6/MoO_3/Ag	16.14	39
2023	ITO/ZnO/PM6:BTP-BO-4Cl:PC61BM/MoO_3/Ag	15.78	40
2023	ITO/Ir/IrOx/PM6:Y6:$PC_{71}BM$/MoO_x/Ag	16.19	41
2023	ITO/ZnO/D18-Cl6:Y6-BO/MoO_3/Ag	16.23	42
2023	ITO/ZnO/PM6:L8-BO/MoO_3/Ag	17.28	43
2023	ITO/ZnO/D18-Cl:3-CITh/MoO_3/Ag	17.30	44
2023	ITO/ZnO/PM6:PBQx-TCl:eC9-2Cl/MoO_3/Ag	17.5	45
2023	ITO/ZnO/PQSi705:m-THE/MoO_3/Ag	18.02	39
2023	ITO/I-MoO_x/PM6:L8-BO/S3-ZnO NPs/Ag	18.9	This work

Table S12. The cost-performance correlations of PEDOT:PSS, I-MoO_x, PFN-Br and S3-ZnO NPs.

Material	Brand	Packing specification	Price (¥)
PEDOT:PSS (Clevios™ P VP Al 4083)	Heraeus	100 mL	1500
PFN-Br	Solarmer	500 mg	2800
100 mL of PFN-Br solution (0.5 mg mL^{-1})			282.8
MAI, 99%	TCI	25 g	1670
MoO_3, 99.9995%	Alfa Aesar	100 g	3826
H_2O_2, 30%	SCR	500 mL	24
100 mL of I-MoO_x solution (10 mg mL^{-1})			46
diethylene glycol monomethyl ether, 98%	Leyan	1000 g	91.2
p-Toluene sulfochloride, 99%	Macklin	1000 g	186.3
KOH, 85.0%	SCR	500 g	32
THF, 99.5%	Greeagent	25 L	1612.5
benzoic acid,4- hydroxy-,ethyl ester, 98.5%	SCR	1000 g	169.6
K_2CO_3, 98%	Aladdin	500 g	41.65
N,N-Dimethylformamide, 99.9%	Anethyst	25 L	1048.5
ethanol	Greagent	25 L	395.25
zinc acetate dihydrate, 98%	Sigma-Aldrich	500 g	933.01
methanol	SCR	500 mL	14
100 mL of S3-ZnO NPs solution (5 mg mL^{-1})			10.85

Reference

1. Y. Tao, H. Liu, D. Wang, F. Zhao, Z. Chen, H. Zhu, H. Chen and C. Z. Li, *InfoMat*, 2022, **4**, e12276.
2. B. Yang, Y. Chen, Y. Cui, D. Liu, B. Xu and J. Hou, *Adv. Energy Mater.*, 2018, **8**, 1800698.
3. Q. Kang, B. Yang, Y. Xu, B. Xu and J. Hou, *Adv. Mater.*, 2018, **30**, e1801718.
4. Z. Zheng, Q. Hu, S. Zhang, D. Zhang, J. Wang, S. Xie, R. Wang, Y. Qin, W. Li, L. Hong, N. Liang, F. Liu, Y. Zhang, Z. Wei, Z. Tang, T. P. Russell, J. Hou and H. Zhou, *Adv. Mater.*, 2018, DOI: 10.1002/adma.201801801, 1801801.
5. L. Lu, Q. Liao, Y. Zu, Y. Xu, B. Xu and J. Hou, *Adv. Energy Mater.*, 2019, **9**, 1803826.
6. B. Guo, Q. Yin, J. Zhou, W. Li, K. Zhang and Y. Li, *ACS Sustainable Chem. Eng.*, 2019, **7**, 8206-8214.
7. M. Zeng, W. Zhu, J. Luo, N. Song, Y. Li, Z. Chen, Y. Zhang, Z. Wang, W. Liang, B. Guo, K. Zhang, F. Huang and Y. Cao, *Sol. RRL*, 2020, **5**, 2000625.
8. Q. Kang, Y. Zu, Q. Liao, Z. Zheng, H. Yao, S. Zhang, C. He, B. Xu and J. Hou, *J. Mater. Chem. A*, 2020, **8**, 5580-5586.
9. H. Xu, H. Zou, D. Zhou, G. Zeng, L. Chen, X. Liao and Y. Chen, *ACS Appl. Mater. Interfaces*, 2020, **12**, 52028-52037.
10. Q. Kang, Z. Zheng, Y. Zu, Q. Liao, P. Bi, S. Zhang, Y. Yang, B. Xu and J. Hou, *Joule*, 2021, **5**, 646-658.
11. J. Yu, X. Liu, Z. Zhong, C. Yan, H. Liu, P. W. K. Fong, Q. Liang, X. Lu and G. Li, *Nano Energy*, 2022, **94**, 106923.
12. Q. Kang, C. Yang, B. Xu and J. Hou, *J. Energy Chem.*, 2022, **69**, 108-114.
13. G. Zhang, Q. Chen, Z. Zhang, J. Fang, C. Zhao, Y. Wei and W. Li, *Angew. Chem. Int. Ed.*, 2023, DOI: doi.org/10.1002/ange.202216304, e202216304.
14. Y. Jiang, X. Dong, L. Sun, T. Liu, F. Qin, C. Xie, P. Jiang, L. Hu, X. Lu, X. Zhou, W. Meng, N. Li, C. J. Brabec and Y. Zhou, *Nat. Energy*, 2022, **7**, 352-359.
15. L. Tan, Y. Wang, J. Zhang, S. Xiao, H. Zhou, Y. Li, Y. Chen and Y. Li, *Adv. Sci.*, 2019, **6**, 1801180.
16. H. Liu, Z. X. Liu, S. Wang, J. Huang, H. Ju, Q. Chen, J. Yu, H. Chen and C. Z. Li, *Adv. Energy Mater.*, 2019, **9**, 1900887.
17. J. Yuan, Y. Zhang, L. Zhou, G. Zhang, H.-L. Yip, T.-K. Lau, X. Lu, C. Zhu, H. Peng, P. A. Johnson, M. Leclerc, Y. Cao, J. Ulanski, Y. Li and Y. Zou, *Joule*, 2019, **3**, 1140-1151.
18. M. Cui, D. Li, X. Du, N. Li, Q. Rong, N. Li, L. Shui, G. Zhou, X. Wang, C. J. Brabec and L. Nian, *Adv. Mater.*, 2020, **32**, e2002973.
19. H. N. Tran, S. Park, F. T. A. Wibowo, N. V. Krishna, J. H. Kang, J. H. Seo, H. Nguyen-Phu, S. Y. Jang and S. Cho, *Adv. Sci.*, 2020, **7**, 2002395.
20. W. Zha, H. Gu, W. Pan, X. Sun, Y. Han, Z. Li, X. Weng, Q. Luo, S. Yang and C.-Q. Ma, *Chem. Eng. J.*, 2021, **425**, 130620.
21. C. Li, X. Zhang, N. Yu, X. Gu, L. Qin, Y. Wei, X. Liu, J. Zhang, Z. Wei, Z. Tang, Q. Shi and H. Huang, *Adv. Funct. Mater.*, 2021, **32**, 2108861.
22. B. Fan, F. Lin, J. Oh, H. Fu, W. Gao, Q. Fan, Z. Zhu, W. J. Li, N. Li, L. Ying, F.

Huang, C. Yang and A. K. Y. Jen, *Adv. Energy Mater.*, 2021, **11**, 2101768.
23. K. Yang, S. Chen, Y. Zhou, G. O. Odunmbaku, Z. Xiong, Q. Yang, M. Wang, Z. Kan, Z. Xiao, S. Lu and K. Sun, *J. Energy Chem.*, 2021, **61**, 141-146.
24. Y. Han, H. Dong, W. Pan, B. Liu, X. Chen, R. Huang, Z. Li, F. Li, Q. Luo, J. Zhang, Z. Wei and C. Q. Ma, *ACS Appl. Mater. Interfaces*, 2021, **13**, 17869-17881.
25. J. Zheng, Y. Luo, X. Wen, Q. Zhang, Y. Song, J. Zhou, N. Jiang, L. Liu, F. Huang and Z. Xie, *J. Mater. Chem. A*, 2021, **9**, 9616-9623.
26. H. Chen, R. Zhang, X. Chen, G. Zeng, L. Kobera, S. Abbrent, B. Zhang, W. Chen, G. Xu, J. Oh, S.-H. Kang, S. Chen, C. Yang, J. Brus, J. Hou, F. Gao, Y. Li and Y. Li, *Nat. Energy*, 2021, **6**, 1045-1053.
27. X. Song, G. Liu, P. Sun, Y. Liu and W. Zhu, *J Phys Chem Lett*, 2021, **12**, 10616-10621.
28. C. Song, X. Huang, T. Zhan, L. Ding, Y. Li, X. Xue, X. Lin, H. Peng, P. Cai, C. Duan and J. Chen, *ACS Appl. Mater. Interfaces*, 2022, **14**, 40851-40861.
29. L. Zeng, L. Zhang, L. Mao, X. Hu, Y. Wei, L. Tan and Y. Chen, *Adv. Opt. Mater.*, 2022, **10**, 2200968.
30. Q. Liao, Q. Kang, Y. Yang, Z. Zheng, J. Qin, B. Xu and J. Hou, *CCS Chem.*, 2022, **4**, 938-948.
31. Y. Huang, L. Meng, H. Liang, M. Li, H. Chen, C. Jiang, K. Zhang, F. Huang, Z. Yao, C. Li, X. Wan and Y. Chen, *J. Mater. Chem. A*, 2022, **10**, 11238-11245.
32. Y. Dong, R. Yu, B. Zhao, Y. Gong, H. Jia, Z. Ma, H. Gao and Z. Tan, *ACS Appl. Mater. Interfaces*, 2022, **14**, 1280-1289.
33. B. Liu, X. Su, Y. Lin, Z. Li, L. Yan, Y. Han, Q. Luo, J. Fang, S. Yang, H. Tan and C. Q. Ma, *Adv. Sci.*, 2022, **9**, e2104588.
34. H. Gao, X. Wei, R. Yu, F. Y. Cao, Y. Gong, Z. Ma, Y. J. Cheng, C. S. Hsu and Z. a. Tan, *Adv. Opt. Mater.*, 2022, **10**, 2102031.
35. S. Li, Q. Fu, L. Meng, X. Wan, L. Ding, G. Lu, G. Lu, Z. Yao, C. Li and Y. Chen, *Angew. Chem. Int. Ed.*, 2022, **61**, e202207397.
36. X. Liu, Z. Zheng, J. Wang, Y. Wang, B. Xu, S. Zhang and J. Hou, *Adv. Mater.*, 2022, **34**, e2106453.
37. R. Yu, X. Wei, G. Wu, T. Zhang, Y. Gong, B. Zhao, J. Hou, C. Yang and Z. a. Tan, *Energy Environ. Sci.*, 2022, **15**, 822-829.
38. Q. Huang, J. Jing, K. Zhang, Y. Chen, A. Song, Z. Liu and F. Huang, *J. Mater. Chem. A*, 2022, **10**, 23973-23981.
39. H. Liu, D. Yuan, H. Jiang, S. Li, L. Zhang and J. Chen, *Energy Environ. Sci.*, 2023, **16**, 3474-3485.
40. L. Sang, X. Chen, J. Fang, P. Xu, W. Tian, K. Shui, Y. Han, H. Wang, R. Huang, Q. Zhang, Q. Luo and C. Q. Ma, *Adv. Funct. Mater.*, 2023, 2304824.
41. Y. Li, B. Huang, X. Zhang, J. Ding, Y. Zhang, L. Xiao, B. Wang, Q. Cheng, G. Huang, H. Zhang, Y. Yang, X. Qi, Q. Zheng, Y. Zhang, X. Qiu, M. Liang and H. Zhou, *Nature Communications*, 2023, **14, 1241**.
42. H. Liu, Z. Zhang, D. Yuan, M. Chen, H. Jiang, J. Liang, X. Chen, D. Sun, L. Zhang, L. Liu, Y. Ma and J. Chen, *J. Mater. Chem. A*, 2023.

43. J. Qin, N. Wu, W. Chen, B. Liu, Z. Wang, L. Zhang, N. Yin, Q. Chen, Z. B. Zhang and C. Q. Ma, *Small Methods*, 2023, **7**, 2300224.
44. B. Fan, W. Gao, R. Zhang, W. Kaminsky, F. R. Lin, X. Xia, Q. Fan, Y. Li, Y. An, Y. Wu, M. Liu, X. Lu, W. J. Li, H.-L. Yip, F. Gao and A. K. Y. Jen, *J. Am. Chem. Soc.*, 2023, **145**, 5909-5919.
45. Y. Yu, Y. Cui, T. Zhang, Z. Chen, Y. Xiao, W. Wang, Y. Yang, N. Yang and J. Hou, *Adv. Funct. Mater.*, 2023, 2306095.